Current Controller for Switched Reluctance Motors Using Pole Placement Approach

M.W. Arab[*], *Student Member, IEEE*, E. Godoy[+], *Member, IEEE*, I. Bahri[*], *Member, IEEE*, M. Hilairet[°], *Member, IEEE*, P. García Estébanez[#] and S. A. Randi[#]

[*]LGEP/SPEE Labs; CNRS UMR8507; SUPELEC; Univ Pierre et Marie Curie-P6; Univ Paris Sud-P11, 91192 Gif sur Yvette, France

[+]Automatic Control Department, Ecole supérieure d'électricité (SUPELEC), F-91192 Gif Sur Yvette Cedex, France

[°]FEMTO-ST, CNRS UMR CNRS 6174, University of Franche-Comte, F-90010 Belfort, France

[#]Technocentre Renault, 1 avenue du Golf, 78288 Guyancourt cedex, France

mohammad-waseem.arab@lgep.supelec.fr, Emmanuel.Godoy@supelec.fr, Imen.Bahri@lgep.supelec.fr, mickael.hilairet@univ-fcomte.fr, pablo.garcia@renault.com, sid-ali.randi@renault.com

Abstract—**This paper presents a design method of a current controller for switched reluctance motors (SRM). The design is carried using pole placement approach which allows taking into consideration the time delays in the open loop transfer function. Also, the tracking dynamics of the controller are enhanced through the integration of a feedforward component. The implementation of an anti-wind up strategy for managing intervals of control signal saturation is then presented. A comparison with a gain-scheduling PI controller reveals a faster response as well as a considerable torque gain at mid-range speeds.**

Index Terms—**Current controller, Feedforward controller, Pole-placement approach, Switched reluctance machine (SRM).**

I. INTRODUCTION

Recently, switched reluctance motors have gained increased interest in both academic and industrial domains. Although invented in the 19th century, their application has only expanded in the last two decades due to advancements in power electronics and digital control. Nowadays, SRMs are being reconsidered for many applications including those of electric mobility due to their numerous advantages such as low production cost and mechanical robustness [1]. Yet, there are still some shortcomings to overcome such as torque ripple and acoustic noise. Different strategies treating these issues were proposed in the literature. Most of these strategies are based on offline optimization of current references with an objective function representing the desired performance. In such case, the current controller plays a major role as it assures the production of this desired performance by means of good tracking of the optimized current reference. Therefore, it becomes essential to study thoroughly the performance of the current regulation loop.

Current control can be challenging at high speed applications as the electrical frequency in SRMs is proportional to the mechanical speed and the number of rotor teeth. This translates to shorter current pulses when the speed increases which imposes the necessity of a faster current response time/higher bandwidth. However, the feasible control bandwidth depends on the choice of the sampling period. In practice, this latter is also limited by the maximum switching frequency of the power converter. In addition, time delays present in the control loop will penalize the controller bandwidth. As a result, regular design methods in continuous time domain might fail to satisfy the needed specifications on current control.

Another problem arises from the nonlinear nature of this type of motors. The phase inductance is a nonlinear expression depending on both the current and the electrical position. In [2], authors propose an adaptive proportional-integral (PI) controller where the gains are calculated online based on the phase inductance value. The inductance is in turn estimated using an analytic expression obtained using Fourier series. In [3], three controllers where compared including a "hybrid" current controller which combines the advantages of both an ON-OFF controller and a PI controller. However, in both studies the tested motor had a considerably inferior DC link voltage and therefore lower current dynamics. Also, the maximum operation speed is four times lower than the prototype studied in this paper which is not very challenging vis-à-vis the required control bandwidth.

In this paper, the proposed controller achieves the desired performance through the choice of the closed loop poles [4]. The design is carried in discrete time domain which allows taking into account time delays due to practical implementation. In order to maintain torque production at mid-range speeds, the current controller tracking dynamics are enhanced through the addition of a feedforward component. The windup problem is presented as well as an effective strategy to overcome this issue. In general, the proposed method proved to be effective in applications where the bandwidth of the controller approaches the limits imposed by the sampling frequency.

This paper is organized as the following: section II addresses the modeling of the SRM. In section III, the design of the controller is presented in details. In section IV, the performance of the proposed controller is demonstrated by means of digital simulation. Finally, a conclusion is presented

in section V.

II. SYSTEM DESCRIPTION AND MODELING

SRMs are by nature nonlinear systems. This is due to the fact that the flux linkage (and therefore the phase inductance L) depends on the phase current and the rotor position [5], [6]. To develop the model of one phase winding we part from (1) which describes the electromagnetic behavior of the latter:

$$u = R_{ph}i + \frac{d\phi(\theta_e, i)}{dt} \qquad (1)$$

Developing (1) results in (2)

$$u = R_{ph}i + L_{inc}\frac{\partial i}{\partial t} + E(\theta_e, i, \omega_e) \qquad (2)$$

with:

$$L_{inc} = \frac{d\phi(\theta_e, i)}{di} \qquad (3)$$

$$E(\theta_e, i, \omega_e) = \omega_e \frac{d\phi(\theta_e, i)}{d\theta_e} \qquad (4)$$

where u is the phase voltage, i is the phase current, R_{ph} is the phase resistance, θ_e and ω_e are respectively the electrical angular position and speed, $\phi(\theta_e, i)$ is the phase flux linkage, L_{inc} is the incremental inductance shown in Fig. 1 and $E(\theta_e, i, \omega_e)$ is the back electromagnetic force (back-emf). The last two terms are calculated offline using finite elements method [7] and stored as 2D lookup tables for online linear interpolation.

Assuming compensation of the back-emf, the system transfer function can be formulated as in (5), which is a symbolic expression.

$$G(s) = \frac{I(s)}{U(s)} = \frac{1}{L_{inc}s + R_{ph}} \qquad (5)$$

For the purpose of controller design, a discrete model corresponding to (5) with an ensemble zero-order hold/sampler can be approximated as (6).

$$G(z^{-1}) = \frac{I(z^{-1})}{U(z^{-1})} = \frac{1}{R_{ph}} \frac{(1-a)z^{-1}}{1 - az^{-1}} \qquad (6)$$

where T_s is the sampling period and $a = e^{-T_s R_{ph}/L_{inc}}$.

This linear discrete model does not represent sufficiently the practical case in which the system is nonlinear. In addition, the implementation of the controller introduces two delay sources that need to be considered for this application:

1) Real-time implementation using a DSP processor presents an output delay of one sample period on the control signal.
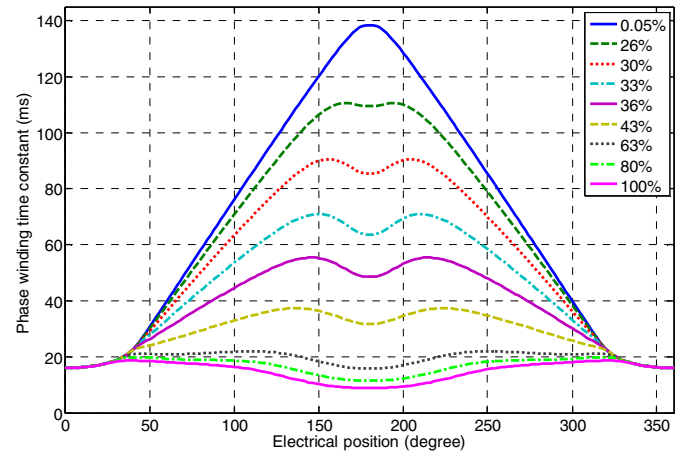

Fig. 1. Phase electrical time constant variation in terms of electrical position and phase current. Phase current indicated as a ratio of the maximum current.

2) The elements of the current measurement loop, such as the anti-aliasing filter or, will introduce phase shifts. In the case of this application, these delays were found to be equivalent to one sample delay.

The aforementioned considerations are included in (6) to give (7) where q represents total sample time delays of the system ($q = 2$):

$$G(z^{-1}) = \frac{1}{R_{ph}} \frac{(1-a)}{1 - az^{-1}} z^{-3} = \frac{B(z^{-1})}{A(z^{-1})} z^{-(q+1)} \qquad (7)$$

III. CONTROLLER DESIGN

In the following section, the current controller design approach in discrete time domain is presented. This controller, denoted in the following as RST controller, is then coupled with a feedforward component to enhance reference tracking dynamics. Finally, an anti-windup strategy is integrated in the controller structure in order to neutralize the effects of control signal saturation intervals. The controller parameters are then determined through an optimization process.

A. RST current controller design

In its general form, an RST controller consists of three polynomials, namely: R, S and T. This structure is shown in Fig. 2. In this structure, a disturbance source was considered on the control signal in order to model the error between the real back-emf and its value deduced through lookup table interpolation. Departing from this structure, the closed loop transfer functions between the two inputs and the output can be found as in (8)

$$Y = \frac{BT}{AS + BR}Y^* + \frac{BS}{AS + BR}V_u$$
$$= G_1(z^{-1})Y^* + G_2(z^{-1})V_u \qquad (8)$$

It can be seen from (8) that the tracking dynamics are influenced by polynomial T whereas those of disturbance

rejection are influenced by polynomial S. This allows decoupling those two dynamics through the design of G_1 and G_2 [8]. For this purpose, the following pre specifications were established on polynomials S and T:

1) In this application, it was found that the back-emf compensation error can be considered as a disturbance of a step form. Equation (9) can be deduced:

$$V_u(z^{-1}) = \frac{V_0}{1 - z^{-1}} \tag{9}$$

where V_0 is the step signal amplitude.

The disturbance rejection model G_2 then becomes:

$$Y = \frac{BS}{AS + BR} V_u = \frac{BS}{AS + BR} \frac{V_0}{1 - z^{-1}} \tag{10}$$

From (10), the disturbance signal influence on the output is represented by its pole in the denominator. Therefore, this pole is compensated by imposing S to be of the form:

$$S(z^{-1}) = (1 - z^{-1})S' \tag{11}$$

this formulation allows canceling the steady state error with respect to the disturbance.

2) In order to obtain a closed loop unity response in steady state, a condition is imposed on polynomial T:

$$T(1) = R(1) \tag{12}$$

Also, the order of this polynomial can be freely chosen by the designer. Therefore, poles of the tracking function G_1 can be compensated to reduce the order of this latter.

Based on the previous pre specifications, R and S are then calculated from the Diophantine equation given as:

$$AS + BR = D(z^{-1}) \tag{13}$$

Pre specification 1 implies:

$$A(1 - z^{-1})S' + BR = A_a S' + BR = D(z^{-1}) \tag{14}$$

where A_a represents the augmented polynomial A, D contains the desired poles of the closed loop.

In order to have a unique solution of (14), three conditions have to be satisfied:

$$\deg(D) \leq \deg(A_a) + \deg(B) + q - 1 \leq 4 \tag{15}$$

$$\deg(S') = \deg(B) + q - 1 \Rightarrow \deg(S') = 2 \tag{16}$$

$$\deg(R) = \deg(A_a) - 1 \Rightarrow \deg(R) = 1 \tag{17}$$

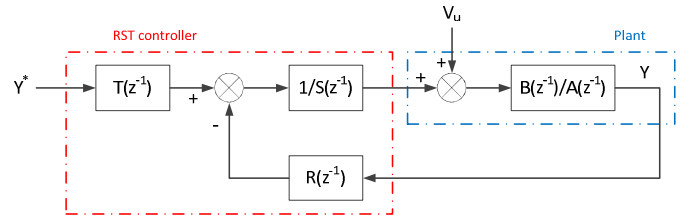We opt for $\deg(D) = 4$. These poles were chosen as in (18):

Fig. 2. General structure of an RST controller.

$$\begin{aligned} c_1 = c_2 = e^{-\omega_{n1}T_e} \\ c_3 = c_4 = e^{-\omega_{n2}T_e} \end{aligned} \tag{18}$$

where c_1, c_2 are the dominant poles. These poles typically have slower dynamics and they have a considerable influence on the response of the system. c_3, c_4 are the auxiliary poles which enhance the disturbance rejection at higher frequencies. Thus, the calculation of polynomial D is carried as given in (19).

$$D = (1 - c_1 z^{-1})(1 - c_2 z^{-1})(1 - c_3 z^{-1})(1 - c_4 z^{-1})$$
$$\tag{19}$$
$$= 1 + d_1 z^{-1} + d_2 z^{-2} + d_3 z^{-3} + d_4 z^{-4}$$

Given D, the matrix form of the Diophantine equation is then given as:

$$\begin{bmatrix} 1 & 0 & 0 & 0 & 0 \\ -(1+a) & 1 & 0 & 0 & 0 \\ a & -(1+a) & 1 & 0 & 0 \\ 0 & a & -(1+a) & (1-a)/R_{ph} & 0 \\ 0 & 0 & a & 0 & (1-a)/R_{ph} \end{bmatrix} \begin{bmatrix} S_0' \\ S_1' \\ S_2' \\ R_0 \\ R_1 \end{bmatrix} = \begin{bmatrix} 1 \\ d_1 \\ d_2 \\ d_3 \\ d_4 \end{bmatrix}$$

The design of polynomial T is based on pre specification 2. Therefore, poles of the tracking closed loop are compensated by T to produce a first order tracking function G_1. Based on the above, the final form of T is given as:

$$T(z^{-1}) = \frac{R(1)}{F(1)} F(z^{-1}) \tag{20}$$

where $F(z^{-1})$ contains poles to be compensated in G_1. Here, it was chosen to be as follows:

$$F(z^{-1}) = (1 - c_1 z^{-1})(1 - c_2 z^{-1})(1 - c_3 z^{-1}) \tag{21}$$

Finally, the robustness of the control law was evaluated using analysis in the frequency domain. For the sake of comparison, the results were compared with those of a gain-scheduling PI controller detailed in [2] that was configured for a second order closed loop with $\xi = 0.85, \omega_0 = 3600$ rad/s. Fig. 3 shows the Nichols chart of the two controllers for a constant value of L_{inc} equal to its average. The stability margins in the two cases are compared in table I which indicates an advantage of the RST controller. It should be noted that classic analysis methods are not suitable in the case

of nonlinear systems. Yet, they can be sufficient for comparison purposes.

TABLE I
STABILITY MARGINS OF THE TWO CONTROLLERS

	RST	Adaptive PI
Gain margin	6.13 dB	5.17 dB
Phase margin	35.7°	25.5°
Delay margin	$3T_s$	$2T_s$
Cutoff frequency	1980 Hz	1920 Hz
Resonance frequency	834 Hz	1080 Hz
Resonance peak gain	4.2 dB	7.3 dB

B. Feedforward controller

Achieving a faster tracking response is necessary at mid-range speeds where the duration of the current pulse could even attain values inferior to the current controller rise time. This will translate into a loss in torque production.

The feedforward control principle relies on the inversion of the system to be controlled. Nevertheless, the modeling imperfections impose the need of a feedback loop. Here, the feedforward controller model was obtained as in (22).

$$FC(S) = G^{-1}(S) = L_{inc}S + R_{ph} \approx L_{inc}S \qquad (22)$$

Equation (22) represents a pure derivative term which is not practically realizable. Therefore, (22) is approximated using a filtered derivative model shown in (23). The discrete model is then obtained using forward Euler approximation as shown in Fig. 4.
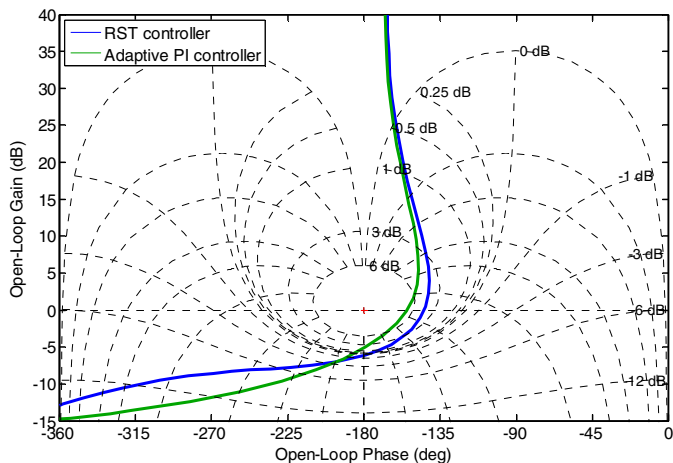
$$FC(S) = \frac{L_{inc}S}{1 + \tau S} \qquad (23)$$

Fig. 3. Nichols chart of the RST and the adaptive PI controller in the case of a constant value of L_{inc}.

C. Anti-windup implementation

In the practical case, the actuator output is limited. This will affect any controller containing an integral component as the integrator state is charged during output saturation intervals. To address this problem in the case of the RST controller, the integral term in polynomial S is isolated as given in (24) in order to allow using classic anti-wind up strategies.

$$\frac{1}{S} = \frac{T_s}{(1 - Z^{-1})} \frac{1}{T_s S'} \qquad (24)$$

In this application, an anti-windup scheme based on feedback of the error between the output and its saturated value was found to give satisfactory results. This scheme is shown in Fig. 5.

D. Parameters optimization

The configuration of the controller parameters can be seen as an optimization problem. For this application, four parameters are to be set, i.e. the closed loop poles pulsations ω_{n1} and ω_{n2}, the feedforward time constant τ and the anti-windup coefficient k_a. In order to study all the possible configurations sufficiently, an optimization algorithm was employed to determine the best set of parameters on low to mid-range operation speeds. The objective function was based on the square of the error between the current and its reference. The produced setting is shown in the table below:

TABLE II
CONFIGURATION OF THE CONTROLLER PARAMETERS

ω_{n1}	7500 rad/s
ω_{n2}	15000 rad/s
τ	0.5 ms
k_a	2000

A block diagram of the proposed controller is given in Fig. 6.

IV. SIMULATION RESULTS

The performance of the proposed controller was tested by simulation using MATLAB/Simulink software suite. The employed machine model is a nonlinear representation obtained by means of finite elements calculation. The obtained simulation results were compared with those of the gain-scheduling PI controller. The two controllers were simulated at speeds of 25, 50 and 100% of Ω_l which is the speed limit after which the current regulation capability is lost due to the increment of the back-emf.

First, the two controllers were tested at 20% of Ω_l for low and high values of current reference. Figs. 7-8 show an advantage for the RST controller in what concerns current tracking. Yet this advantage does not result in a torque gain as torque production during current rise is not significant. This however does not undermine the benefit of the RST controller as the reference tracking can be vital for other performance
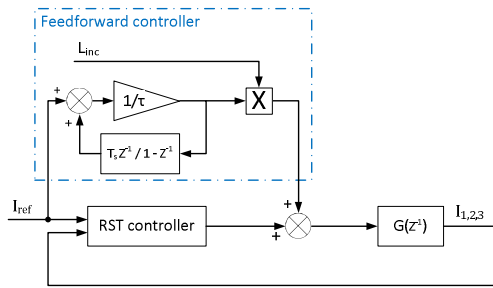
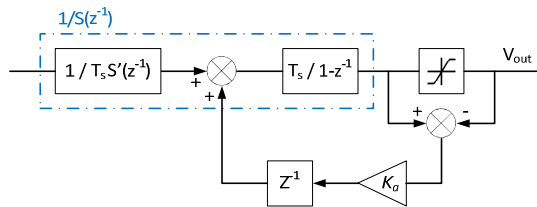Fig. 4. Feedforwad controller in discrete time.
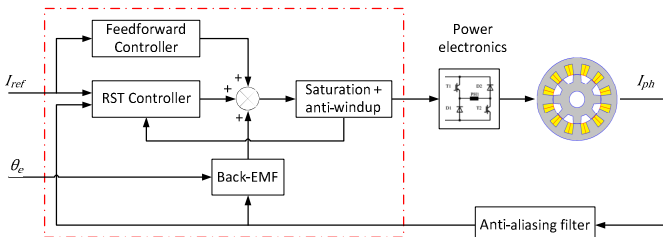

Fig. 5. Anti-windup implementation

Fig. 6. Block diagram of the proposed control law

criteria such as the minimization of losses in the converter or acoustic noise cancellation. The same test was carried at 50% of Ω_l as shown in Figs. 9-10 where the same observations can be made.

At Ω_l, the torque production advantage can be clearly noticed. As shown in Figs. 11 and 12, a torque gain of 230% and 360% are seen for current references of 25% and 100% of I_{max} respectively.

Fig. 13 shows the feedforward component effect on the current reference tracking. As noticed, without this component the current reference tracking is degraded as well as a torque loss of about 16%.

As a final test, the influence of the anti-windup strategy is demonstrated at 4000 RPM. At this speed, the output voltage saturates due the high value of the back-emf. Disabling the anti-windup loop results in current overshoot as the integrator is not discharge effectively, as shown in Fig. 14.
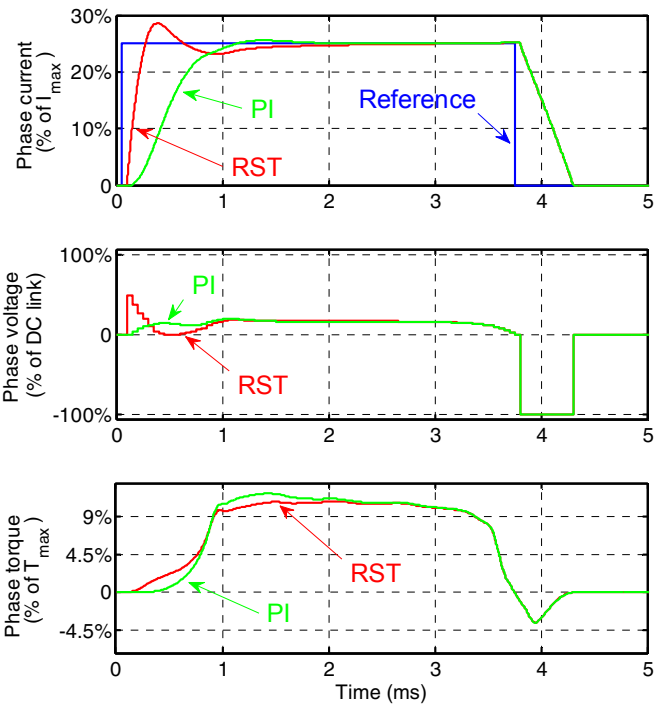

Fig. 7. Simulation at 25% Ω_l, $I^* = 25\%$ I_{max}. Average torque phase (RST) = 4% T_{max}, Average torque per phase (PI) = 4% T_{max}.
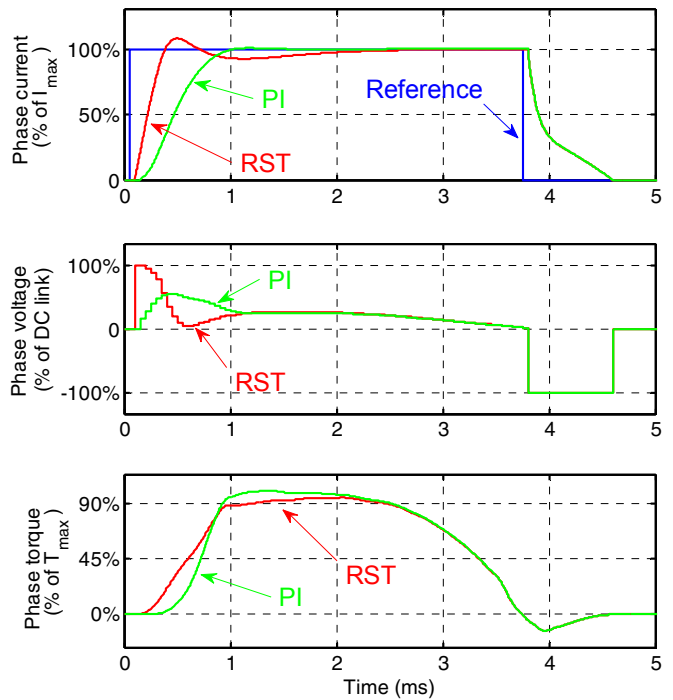

Fig. 8. Simulation at 25% Ω_l, $I^* = 100\%$ I_{max}. Average torque phase (RST) = 32% T_{max}, Average torque per phase (PI) = 32% T_{max}.
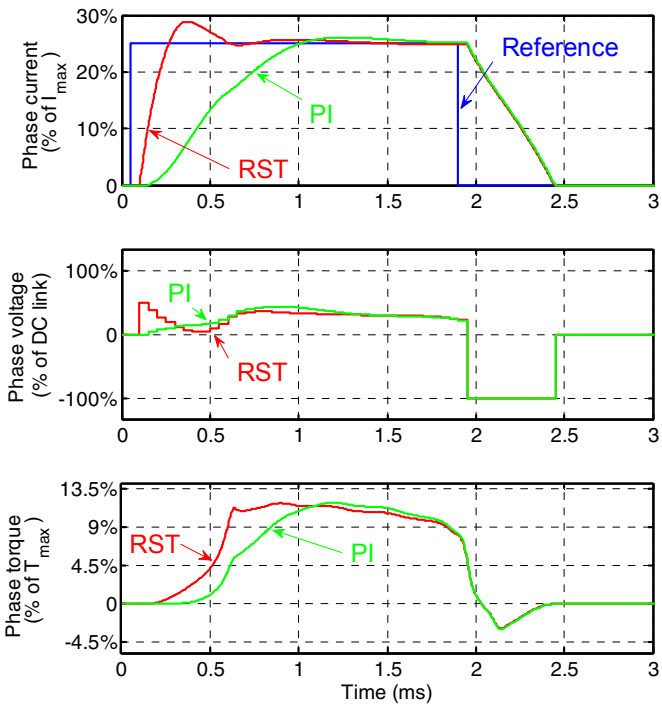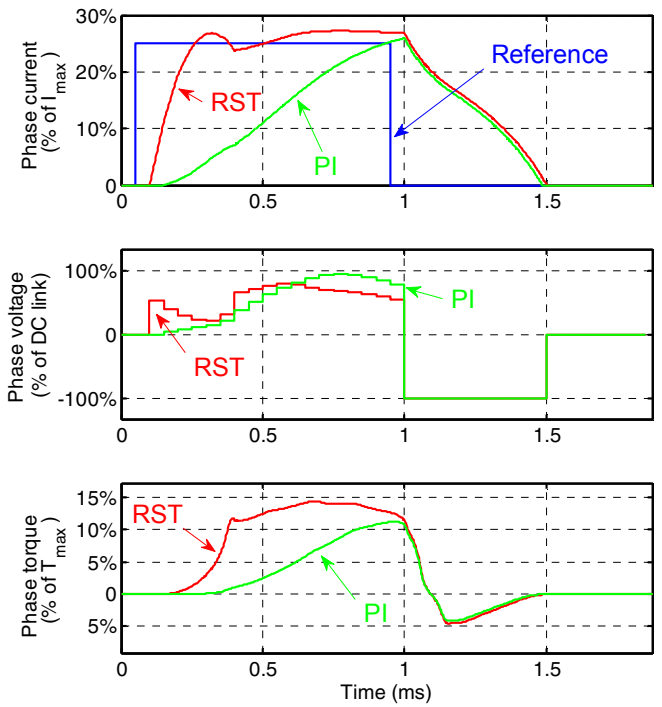
Fig. 9. Simulation at 50% Ω_l, $I^* = 25\%$ I_{max}. Average torque phase (RST) = 4% T_{max}, Average torque per phase (PI) = 3.5% T_{max}.

Fig. 11. Simulation at 100% Ω_l, $I^* = 25\%$ I_{max}. Average torque phase (RST) = 4.4% T_{max}, Average torque per phase (PI) = 1.9% T_{max}.
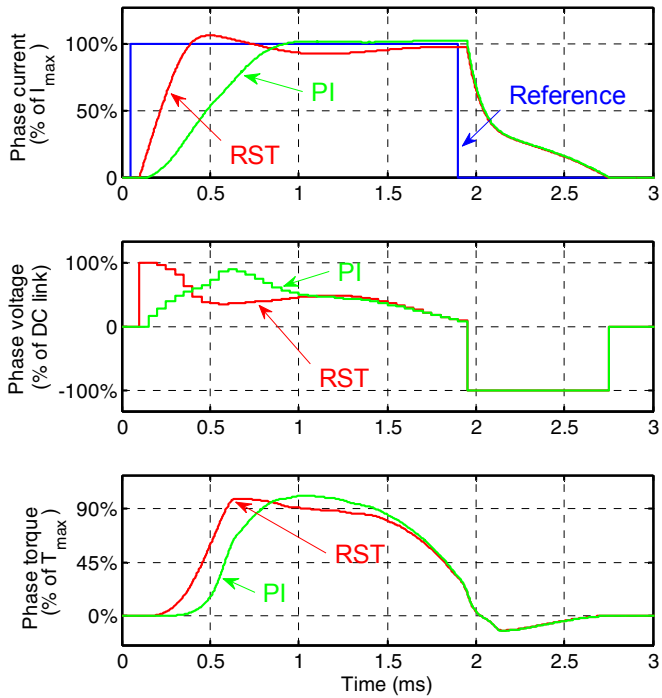

Fig. 10. Simulation at 50% Ω_l, $I^* = 100\%$ I_{max}. Average torque phase (RST) = 32% T_{max}, Average torque per phase (PI) = 30% T_{max}.
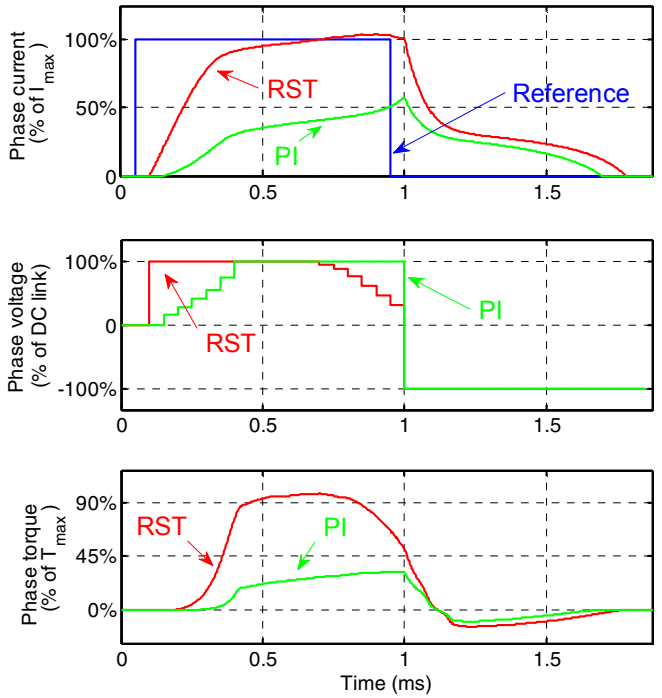

Fig. 12. Simulation at 100% Ω_l, $I^* = 100\%$ I_{max}. Average torque phase (RST) = 32% T_{max}, Average torque per phase (PI) = 8.7% T_{max}
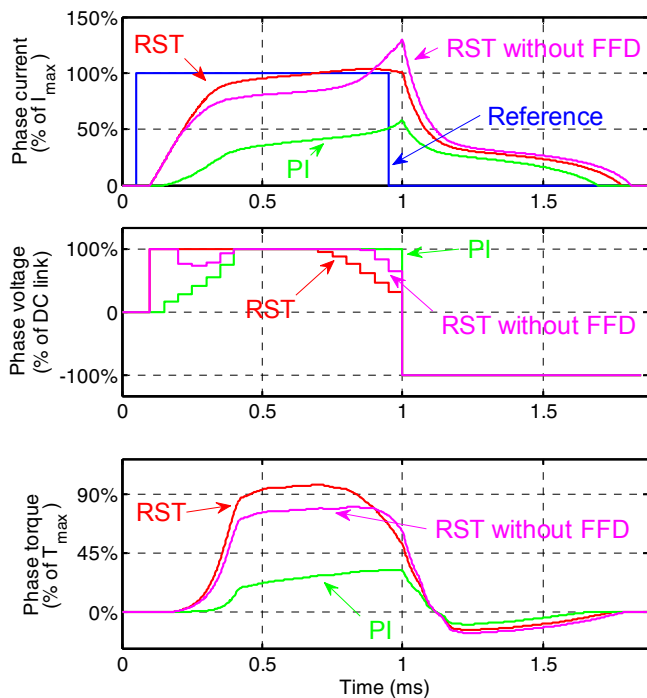
Fig. 13. Simulation at 100% Ω_l, $I^* = 100\% I_{max}$. Average torque phase (RST) = 32% T_{max}, Average torque per phase (PI) = 26.6% T_{max}, Average torque per phase (PI) = 8.7% T_{max}
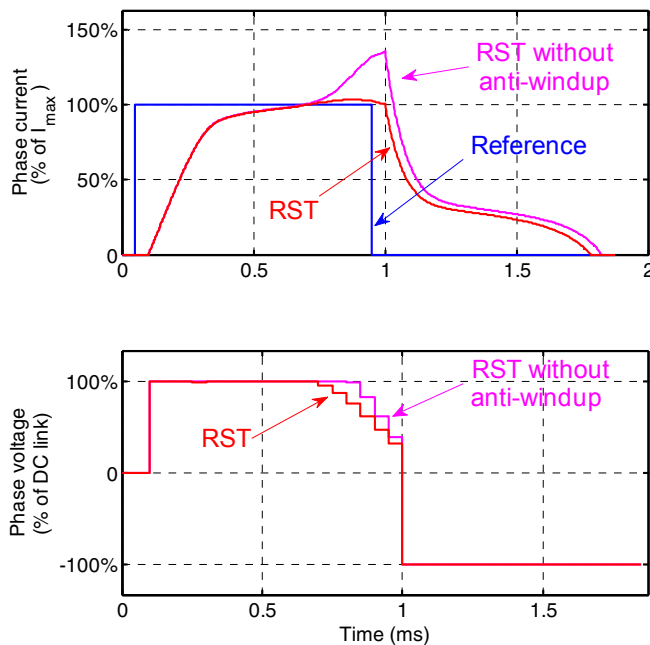

Fig. 14. Simulation at 100% Ω_l, $I^* = 100\% I_{max}$. with and without integrator anti-windup.

V. Conclusion

In this paper, authors have proposed an adaptive RST current controller for switched reluctance motors. A polynomial approach taking into consideration time delays present in the control loop was adopted. Also, the machine nonlinearities were neutralized through online adaptation of the controller's polynomials calculation. To improve the closed loop dynamics, a feedforward component was integrated along with the main controller. Simulation results, using a nonlinear model, have shown that the proposed design approach allows obtaining the desired performances even in the presence of time delays in the control loop. The validation of the control law was performed by means of simulation for low and average speed values. Its efficiency was demonstrated in terms of torque generation. It was shown that the feedforward component has an important role in accelerating the response time of the controller at average speeds.

References

[1] S. Faid, P. Debal, and S. Bervoets, "Development of a Switched Reluctance Motor for Automotive Traction Applications," in *The 25th World Battery, Hybrid and Fuel Cell Electric Vehicle Symposium & Exhibition*, 2010, pp. 5–9.

[2] H. Hannoun, M. Hilairet, and C. Marchand, "High performance current control of a switched reluctance machine based on a gain-scheduling PI controller," *Control Engineering Practice*, vol. 19, no. 11, pp. 1377–1386, Nov. 2011.

[3] X. Rain, M. Hilairet, and O. Bethoux, "Comparative study of various current controllers for the switched reluctance machine," in *2010 IEEE Vehicle Power and Propulsion Conference*, 2010, pp. 1–6.

[4] E. Ostertag and E. Godoy, "RST-Controller Design for Sinewave References by Means of an Auxiliary Diophantine Equation," in *Proceedings of the 44th IEEE Conference on Decision and Control*, 2005, pp. 6905–6910.

[5] R. B. Inderka and R. W. De Doncker, "High-dynamic direct average torque control for switched reluctance drives," *IEEE Transactions on Industry Applications*, vol. 39, no. 4, pp. 1040–1045, Jul. 2003.

[6] N. H. Fuengwarodsakul, M. Menne, R. B. Inderka, and R. W. De Doncker, "High-Dynamic Four-Quadrant Switched Reluctance Drive Based on DITC," *IEEE Transactions on Industry Applications*, vol. 41, no. 5, pp. 1232–1242, Sep. 2005.

[7] M. Besbes and B. Multon, "MRVSIM Logiciel de simulation et d'aide à la conception de Machines à réluctance variable à double saillance à alimentation électronique." CNRS, 2004.

[8] M. Khanchoul and M. Hilairet, "Design and comparison of different RST controllers for PMSM control," in *IECON 2011 - 37th Annual Conference of the IEEE Industrial Electronics Society*, 2011, pp. 1795–1800.